

Article

Mechanochemical Synthesis of High-Entropy Layered Double Hydroxide MgCoNi/AlFeY

Olga Kokoshkina, Maksim Yapryntsev and Olga Lebedeva * 

Department of General Chemistry, Institute of Pharmacy, Chemistry and Biology, Belgorod State National Research University, Belgorod 308015, Russia; nestroynaya@bsuedu.ru (O.K.); yaprintsev@bsuedu.ru (M.Y.)

* Correspondence: olebedeva@bsuedu.ru

Abstract: In the present study, the possibility of synthesizing high-entropy hexacationic layered double hydroxide MgCoNi/AlFeY via mechanochemical synthesis was demonstrated. In the synthesis, the activation rate, activation time, and NaOH amount were varied. The main synthesis stages were as follows: the mechanical activation of salts, NaOH addition, washing with distilled water before achieving neutral pH, and drying at 100 °C. The stage of aging in aqueous solution was omitted. During the synthesis, the activation conditions were varied, the activation time ranged from 1 to 120 min, the rotation speed of the ball mill was changed from 200 to 400 rpm, and the ratio values of sodium hydroxide weight to the mass of cations were specified as 1.0, 1.5, or 2.0. The samples were characterized by X-ray diffraction, transmission electron microscopy, scanning electron microscopy combined with an energy-dispersive analyzer, thermal analysis, Fourier transform infrared spectroscopy, and Raman spectroscopy. The following optimal synthesis conditions for obtaining single-phase sample were determined: an activation rate of 300 rpm, an activation time of 30 min, and an m(cation)-to-m(NaOH) ratio of 1:1.

Keywords: layered double hydroxides; mechanochemical synthesis; high entropy; sorption; photodestruction



Academic Editor: Antonio Polimeni

Received: 9 December 2024

Revised: 19 January 2025

Accepted: 27 January 2025

Published: 2 February 2025

Citation: Kokoshkina, O.; Yapryntsev, M.; Lebedeva, O. Mechanochemical Synthesis of High-Entropy Layered Double Hydroxide MgCoNi/AlFeY. *Solids* **2025**, *6*, 5. <https://doi.org/10.3390/solids6010005>

Copyright: © 2025 by the authors. Licensee MDPI, Basel, Switzerland. This article is an open access article distributed under the terms and conditions of the Creative Commons Attribution (CC BY) license (<https://creativecommons.org/licenses/by/4.0/>).

1. Introduction

Over the past 20 years, high-entropy materials have emerged as one of the most promising areas of research. The concept of high-entropy materials is based on the idea that the presence of five or more components can create single-phase compounds or alloys with unique and emergent properties. The fundamental goal of these materials is to maximize configurational entropy (to minimize Gibbs free energy), thus stabilizing the system for improved reliability and tenability [1,2].

Initially, high-entropy alloys garnered significant attention and contributed greatly to advancements in metallurgy. However, the range of high-entropy compounds has expanded significantly and now includes oxides [3], nitrides [4], sulfides [5], borides [6], and more. The first publication that focused on high-entropy layered double hydroxides (LDHs) appeared in 2020 [7].

Layered double hydroxides are either natural or synthetic compounds characterized by a distinctive layered structure. The general formula for LDHs is $[M_{1-x}^{2+}M_x^{3+}(\text{OH})_2]^{x+}[A^{n-}]_{x/n} \cdot y\text{H}_2\text{O}]^{x-}$, where M^{2+} and M^{3+} represent metal cations surrounded by hydroxyl groups. These metal hydroxocomplexes form brucite-like layers, while the anions (A^{n-}) occupy interlayer spaces, compensating for the positive charge of the brucite layers [8,9]. The structure of layered double hydroxides is notably resistant to variations in the sizes and

quantities of cations and anions, which facilitates their diverse applications. Depending on their composition, LDHs are used in various roles, including as catalysts [10–12], sorbents [13–15], drug carriers [16–18], and electrode materials [7,19,20].

Layered double hydroxides were primarily synthesized through co-precipitation at constant or variable pH levels. Recently, methods such as hydrothermal, microwave, and mechanochemical syntheses have been applied to produce LDHs [21–26].

Mechanochemical synthesis is a promising approach for creating layered double hydroxides. In our research, we explored the synthesis of high-entropy hexacationic layered double hydroxides using the mechanochemical method, starting directly from the corresponding metal salts without an additional aging stage. During this synthesis, we varied the activation conditions, including the activation time, the rotation rate of the ball mill, and the amount of sodium hydroxide used.

2. Materials and Methods

MgNiCo/AlFeY layered double hydroxides (LDHs) were synthesized using a mechanochemical method. The initial reagents included sodium hydroxide (NaOH) and the following salts: magnesium nitrate ($\text{Mg}(\text{NO}_3)_2 \cdot 6\text{H}_2\text{O}$), nickel nitrate ($\text{Ni}(\text{NO}_3)_2 \cdot 6\text{H}_2\text{O}$), cobalt(II) nitrate ($\text{Co}(\text{NO}_3)_2 \cdot 6\text{H}_2\text{O}$), aluminum nitrate ($\text{Al}(\text{NO}_3)_3 \cdot 9\text{H}_2\text{O}$), iron(III) nitrate ($\text{Fe}(\text{NO}_3)_3 \cdot 9\text{H}_2\text{O}$), and yttrium nitrate ($\text{Y}(\text{NO}_3)_3 \cdot 6\text{H}_2\text{O}$). The molar ratio of M(II) to M(III) was 3:1. The precalculated cationic composition of the LDH was $\text{Mg}_{15}\text{Co}_{15}\text{Ni}_{45}/\text{Al}_{20}\text{Fe}_{2.5}\text{Y}_{2.5}$.

The synthesis was conducted in a planetary ball mill (FRITSCH Pulverisette 6) equipped with a grinding jar containing 40 grinding balls (with a 500 mL volume, 10 mm diameter, and 13.5 g weight) made of stainless steel. Powders of salts (540 g in total) were placed in the grinding jar, and the mixture was activated for a specified time. Following this, sodium hydroxide was added and the stirring continued. The activation time ranged from 1 to 120 min, with the rotation speed of the ball mill set between 200 and 400 rpm. The ratio of sodium hydroxide concentration to cation concentration was adjusted to 1, 1.5, or 2 in the different experiments. The resulting viscous paste was transferred to a beaker and washed with distilled water until a neutral pH was achieved. The sample was then dried at 100 °C for 3 h. Notably, the typical aging stage of LDHs under the mother liquor was omitted.

The structure and phase composition of the synthesized samples were characterized using X-ray diffraction (XRD) on a Rigaku Ultima IV diffractometer with $\text{CuK}\alpha$ radiation. The scanning range was 5–80° (2 θ) with a step size of 0.02° and a rate of 2°/min. Phase composition analysis was performed using standard techniques, including registration, LPA correction, background alignment and subtraction, $\text{K}\alpha$ -line subtraction, profile analysis, and database phase search and identification using the powder X-ray standards PDF (JCPDS ICDD) and PDF-2. Crystal structures were identified via PDXL software version 1.8.0.3 (Rigaku, Japan).

Elemental composition data for the synthesized samples were obtained using a high-resolution scanning electron microscope (QUANTA 200 3D FEI) equipped with an energy-dispersive spectrometer, operating at 20 kV.

Morphological studies of the synthesized samples were conducted using transmission electron microscopy (a JEOL JEM-2100 microscope with an accelerating voltage of 200 kV, a resolution of 0.2 nm, and a magnification range of 500 to 1500 times). Sample preparation involved grinding the samples to a powder, dispersing them in acetone under ultrasound guidance, and then applying them to a carbon film.

Thermal transformations of the synthesized materials were examined using a ZCT-H synchronous thermal analysis device from Beijing Jing Yi GAO Ke Instrument Co. Mass changes and thermal effects were analyzed in the temperature range of 30 °C to 900 °C,

with a heating rate of 10 °C/min. The samples were heated in a nitrogen atmosphere within a corundum crucible.

Raman spectra were recorded on a LabRam HR Evolution Raman confocal microspectrometer (HORIBA Jobin Yvon S.A.S., Japan), using a Nd:YAG laser with a wavelength of 532 nm, covering the range from 200 to 2000 cm^{-1} . Fourier transform infrared (FTIR) spectroscopy was performed on an FSM 2201 FTIR spectrometer (Infraspek LLC, Russia) in the range of 500 to 4000 cm^{-1} . Sample preparation involved pressing a mixture of the synthesized sample with potassium bromide in a 100:1 ratio.

The sorption capacity of the MgCoNi/AlFeY series samples was evaluated with respect to the anionic dye methyl orange (MO). Changes in the optical density of the aqueous solutions were measured using a Specord 50 UV/vis spectrometer (Analytik, Jena, Germany), with the optical density recorded at a wavelength of 505 nm. Sorption kinetics was studied at an ambient temperature (20 °C).

The photocatalytic activity of the samples was assessed through the photodegradation of methyl orange dye. The kinetics of the photodegradation reaction was studied in a photolysis chamber (FK-12m, Volta, Russia) equipped with a 1000 W mercury lamp, emitting light in the 240–320 nm range. A total of 50 mg of LDHs was dispersed in 50 mL of the aqueous solution containing 50 mg of the dye and subjected to UV radiation.

3. Results and Discussions

3.1. Influence of Mechanochemical Parameters on the Phase Composition of LDHs

The initial experiments examined the influence of activation time and activation rate on the crystallinity and phase composition of the resulting samples. Additionally, the amount of NaOH was varied.

Powder X-ray diffraction (XRD) patterns of MgCoNi/AlFeY samples, synthesized with different activation rates, times, and amounts of NaOH, are presented in Figure 1a–c, respectively. Figure 1d illustrates the XRD pattern of the nitrate mixture immediately after activation and before the addition of NaOH. It is evident that following activation, a mixture of nitrates, oxides, and mixed oxides forms, making it challenging to attribute all reflections to specific compounds (Figure 1d). However, the addition of sodium hydroxide to the mixture leads to the formation of a structure corresponding to layered double hydroxides (LDHs). The diffraction patterns of all samples synthesized under varying conditions contain typical basal reflections for Mg/Al LDHs (JCPDS card #14-0191), although these reflections are broadened. This may suggest a low degree of crystallinity in the synthesized materials, as well as the potential formation of different LDH polytypes.

The results from the X-ray phase analysis indicated that changing the activation rate from 200 to 400 rpm in the synthesis of hexacationic LDHs does not significantly impact the outcome (Figure 1a). In the XRD patterns, there was no notable variation in reflection intensity with an increase in the activation rate. The samples obtained at activation rates of 200 and 300 rpm exhibited comparable intensity values and peak widths. However, an activation rate of 400 rpm resulted in decreased intensity. Consequently, an activation rate of 300 rpm was chosen for further syntheses.

When varying the activation time, the sample activated for thirty minutes displayed intense reflections in the XRD pattern. Activation beyond 30 min led to a decrease in crystallinity, as demonstrated by diminished reflection intensity. Based on this observation, 30 min was determined to be the optimal activation time.

The observed effects reflect the specificity of mechanochemical synthesis, during which there is always a competition between the disintegration and aggregation of substance particles. As a rule, at the initial stages, the reagents are ground with a decrease in particle size; then, a period of active interaction starts, after which the disintegration of the product

becomes dominant. In our case, the activation time of 30 min approximately corresponds to the beginning of the intensive processes of grinding and the disintegration of LDHs. An increase in the activation rate shortens this period. Thus, an overly high activation rate or prolonged activation is an excessive action and leads to a decrease in the crystallinity of the product that is already formed.

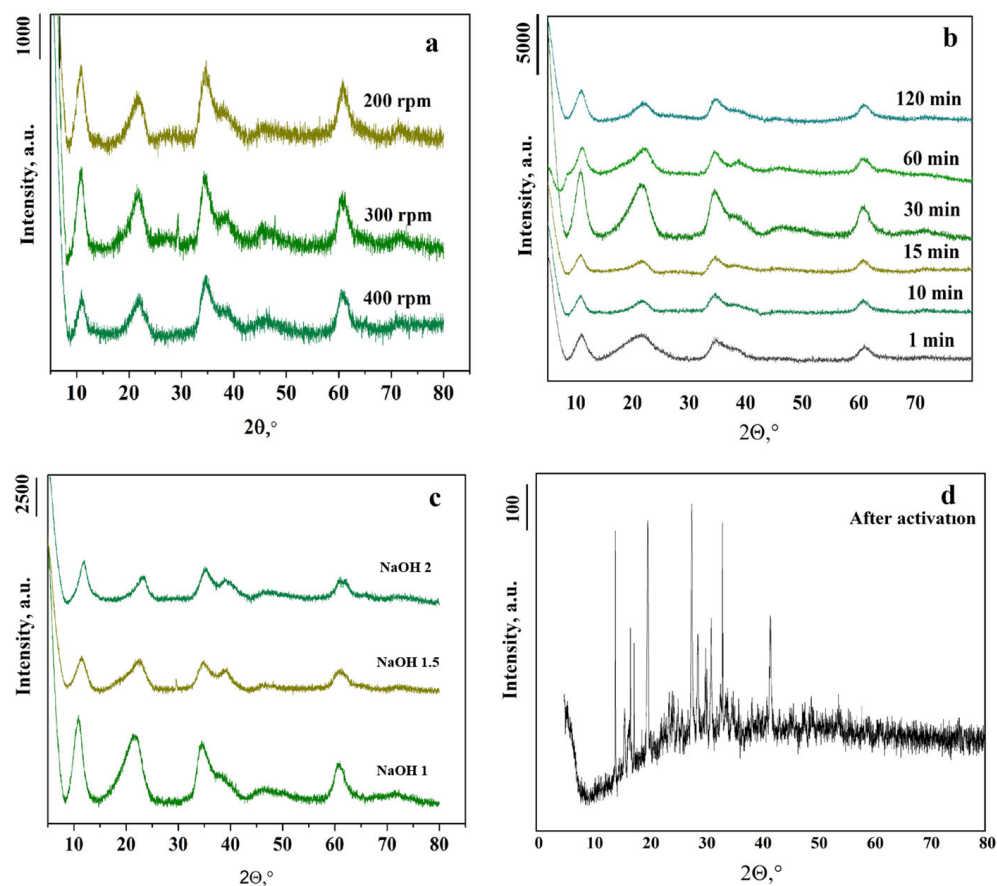


Figure 1. Powder X-ray diffraction patterns of (a) MgCoNi/AlFeY-LDHs obtained with different activation rates; (b) MgCoNi/AlFeY-LDHs obtained with different activation times; (c) MgCoNi/AlFeY-LDHs obtained with different NaOH molar concentrations; and (d) the mixture of original salts after activation.

In the traditional co-precipitation synthesis of LDHs, alkali serves the function of precipitate formation, making excess alkali crucial for LDH structure development. However, in mechanochemical synthesis using crystallohydrates as reactants, the process occurs in a pasty environment resembling a solid-state reaction. The investigation into the effect of NaOH amount on LDH formation revealed that, unlike the co-precipitation method, there is no requirement for excess alkali in the mechanochemical synthesis of hexacationic LDHs. XRD analysis indicates that the most intense reflections originated from the sample synthesized without excess of NaOH (Figure 1c). Moreover, there is no need for an aging stage. This meets the wastewater reduction requirements of green chemistry.

Thus, the optimal conditions for synthesizing hexacationic LDHs of the Mg-CoNi/AlFeY composition were identified: an activation rate of 200 rpm, an activation time of 30 min, and an equimolar ratio of NaOH to the sum of cations. Further characterization was conducted using the sample synthesized under these optimal conditions.

The EDAX spectrum of the optimal LDH sample showed no signs of impurity elements (Figure 2). Instead, the spectrum displayed signals for all the planned and expected elements of the synthesized MgCoNi/AlFeY-LDHs. Notably, there were no signals indicat-

ing the presence of sodium, which confirms the success of the washing stage of the sample. Based on the EDAX results, we calculated the elemental composition and the M^{2+}/M^{3+} ratio. Table 1 presents the values of the atomic fractions of the metal cations and the molar ratio M^{2+}/M^{3+} . The data indicate that the molar ratio M^{2+}/M^{3+} and the atomic fraction values differ slightly from those specified during the synthesis.

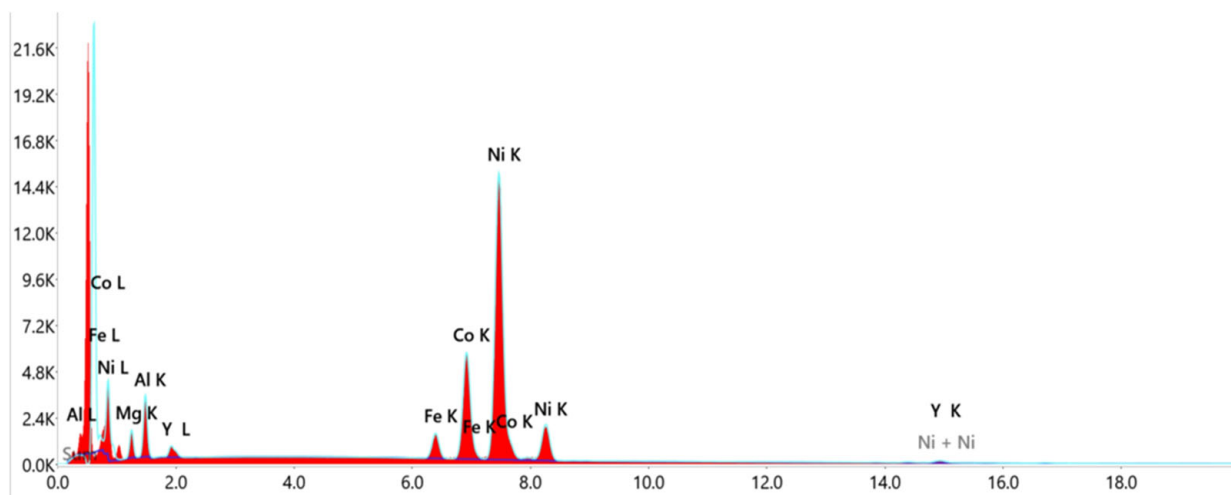


Figure 2. EDAX spectra of MgCoNi/AlFeY-LDHs.

Table 1. Atomic fractions of metal cations and M^{2+}/M^{3+} ratios calculated from the results of EDAX.

	Cationic Fractions, at. %						M^{2+}/M^{3+}
	Ni ²⁺	Co ²⁺	Mg ²⁺	Al ³⁺	Fe ³⁺	Y ³⁺	
Precalculated composition	45.0	15.0	15.0	20.0	2.5	2.5	3.0
Experimental composition	45.0	15.0	15.0	22.0	2.4	1.1	2.9

3.2. Study of Particle Morphology

The morphology of MgCoNi/AlFeY particles synthesized through mechanochemical synthesis was examined using transmission electron microscopy (TEM). The TEM image of the sample is shown in Figure 3a. It reveals several plate-like particles with a hexagonal shape, which is characteristic of layered double hydroxides (LDHs). The synthesized sample displays moderate crystallinity, a finding that is consistent with the previously discussed X-ray diffraction (XRD) data.

Additionally, the elemental mapping of the sample indicates a uniform distribution of all metals across the synthesized material (shown in Figure 3b). This evidence supports the conclusion that a new individual substance has formed rather than a mere mechanical mixture.

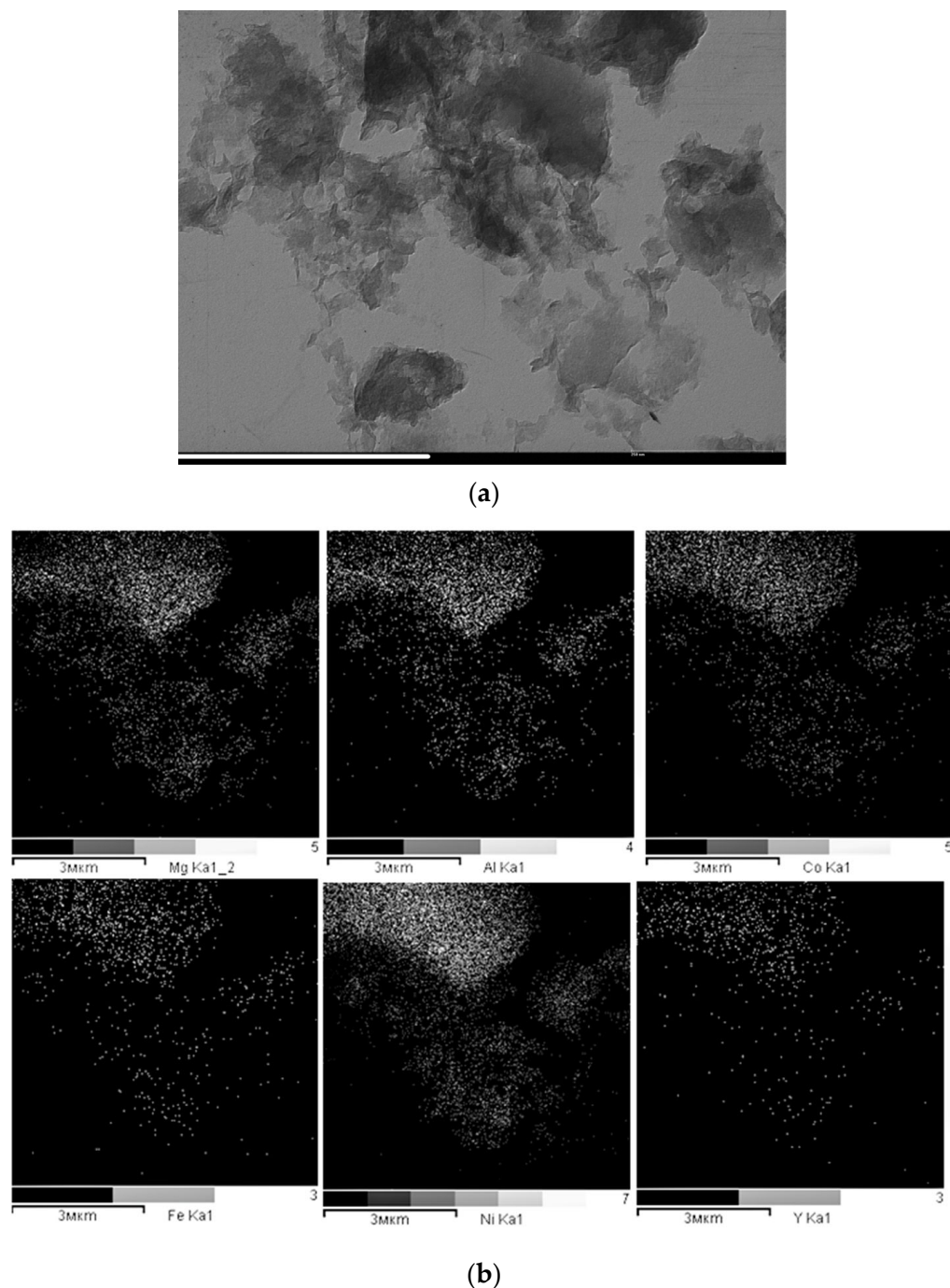


Figure 3. SEM micrographs (a) and elemental distribution maps (b) of MgCoNi/AlFeY-LDHs.

3.3. Study of Thermal Stability

Figure 4 shows the TG curve of the MgCoNi/AlFeY-LDH sample. The curve reveals two main stages of mass loss. The first stage occurs between 100 °C and 250 °C, while the second stage spans from 250 °C to 900 °C. The first stage is associated with the release of adsorbed and interlayer water. The second mass loss is linked to the dehydroxylation of the brucite-like layer, along with the release and breakdown of anions from the interlayer space. Overall, the total mass loss observed is approximately 40%.

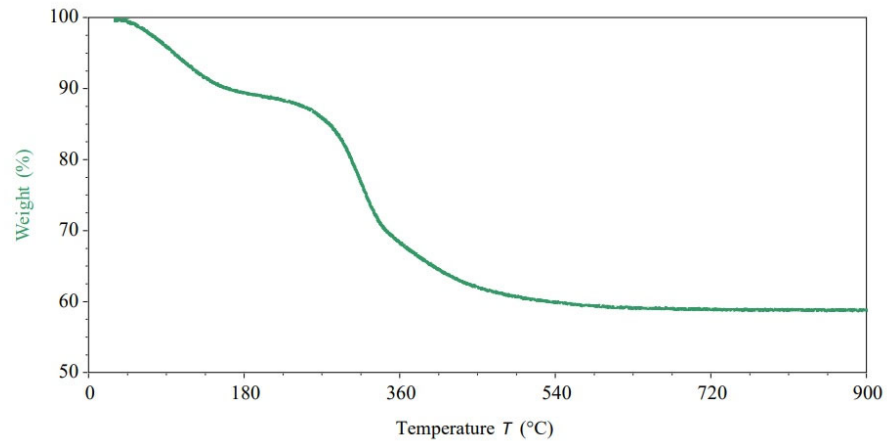


Figure 4. DTA-TG curves of the MgCoNi/AlFeY-LDH sample.

3.4. Characterization of LDHs Using FTIR and Raman Spectroscopy

The IR spectrum of the sample exhibits a typical pattern characteristic of layered double hydroxide (LDH) compounds (Figure 5a). In the region of 3700 to 3300 cm^{-1} , there is a broad band with a maximum at 3440 cm^{-1} , which is attributed to the vibrations of hydroxyl groups in brucite-like layers, as well as water molecules that are interlayered or adsorbed. A prominent signal in the range of 1600 to 1645 cm^{-1} corresponds to the deformation vibrations of the interlayer water.

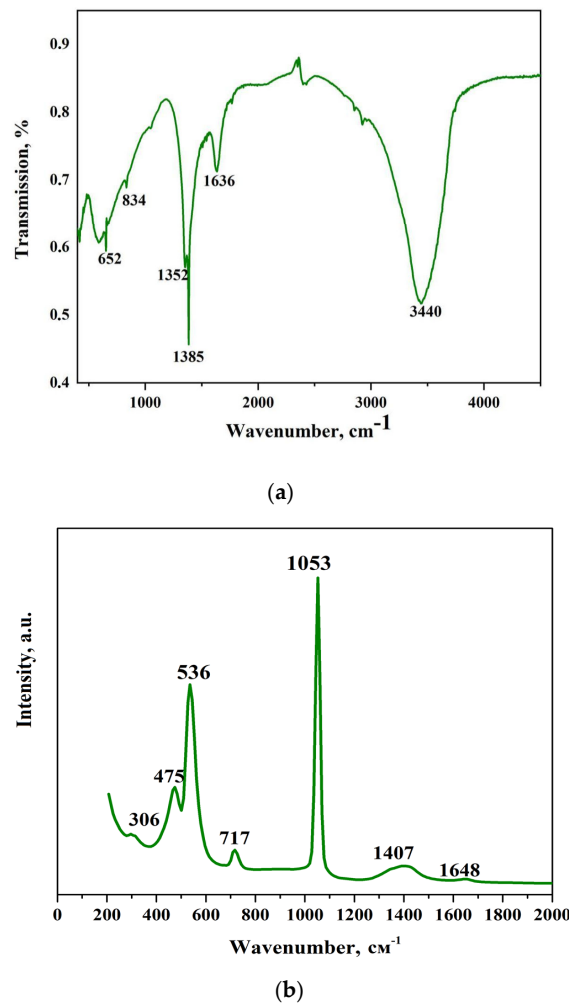


Figure 5. FTIR (a) and Raman (b) spectra of MgCoNi/AlFeY-LDHs.

Additionally, an absorption band was observed in the range of 1440 to 1340 cm^{-1} , which is related to the stretching vibrations of nitrate anions. The spectrum also displays absorption bands in the region below 1000 cm^{-1} , corresponding to Me-O vibrations within the crystal lattice of the sample.

Further insights were obtained through Raman scattering spectroscopy. A band with a maximum at 536 cm^{-1} was observed, which corresponds to the stretching vibrations of Me-O-Me bonds, a distinctive feature of layered double hydroxides. Bands at 717 cm^{-1} , 1070 cm^{-1} , and 1400 cm^{-1} correspond to anions intercalated in the interlayer space, specifically nitrate anions (see Figure 5b).

3.5. Calculation of Configurational Entropy

The calculation of the configurational entropy for the synthesized samples allowed us to evaluate whether the obtained sample can be classified as a high-entropy compound. According to the authors [27], it is essential to consider the number of possible configurations of the structural elements when calculating the configurational entropy of compounds with complex compositions. The threshold value for configurational entropy that classifies compounds as high-entropy is 1.5 R.

We used the following formula to calculate the configurational entropy:

$$\Delta S_{conf} = -R \sum_{i=1}^N x_i \ln x_i \quad (1)$$

where x_i represents the mole fractions of the constituent elements. This formula was proposed in the publication [27]. It can be seen that the configurational entropy depends solely on the composition of the substance, while the method of obtaining it does not affect the value of entropy. It is also worth underlining that only multicomponent LDHs can be highly entropic. The formula shows that the entropy of 2–4-cationic samples cannot reach the threshold value of 1.5 R.

The calculated entropy value for the synthesized sample, considering only the cationic composition of the layered double hydroxide, is 1.43R kJ/mol·K. However, the synthesized material also contains anions (OH^- and NO_3^-). The contributions of each of these anions and the microstates they form are sufficient to exceed the threshold value. Therefore, we can classify the synthesized materials as high-entropy LDHs.

3.6. Study of Sorption and Photocatalytic Properties

The process of anion sorption via layered double hydroxides (LDHs) occurs through various mechanisms. Sorption can take place on the surface of the LDH or through ion exchange, where interlayer anions are replaced by anions from the solution. These processes can happen simultaneously or sequentially. High configurational entropy was not expected to influence either the adsorption value or adsorption kinetics. The study of adsorption served, in our opinion, as a kind of test for the homogeneity of the obtained LDHs.

The kinetic curve for the sorption of methyl orange (MO), as shown in Figure 6, reveals a sharp increase in the amount of MO adsorbed at the initial stage. This suggests a rapid transfer of MO from the solution to the sorption sites on the sample's surface. It is likely that the process begins with surface sorption and is eventually followed by anion exchange. The sample exhibits a moderate sorption capacity for MO.

The kinetic curve was analyzed by applying the Lagergren pseudo-first-order model (Equation (2)) [28] and the Ho and McKay pseudo-second-order model (Equation (3)) [29]. The results are plotted in Figures 7 and 8.

$$\ln(A_e - A_t) = \ln A_e - k_1 t \quad (2)$$

$$\frac{t}{A_t} = \frac{1}{k_2 A_e^2} + \frac{t}{A_e} \tag{3}$$

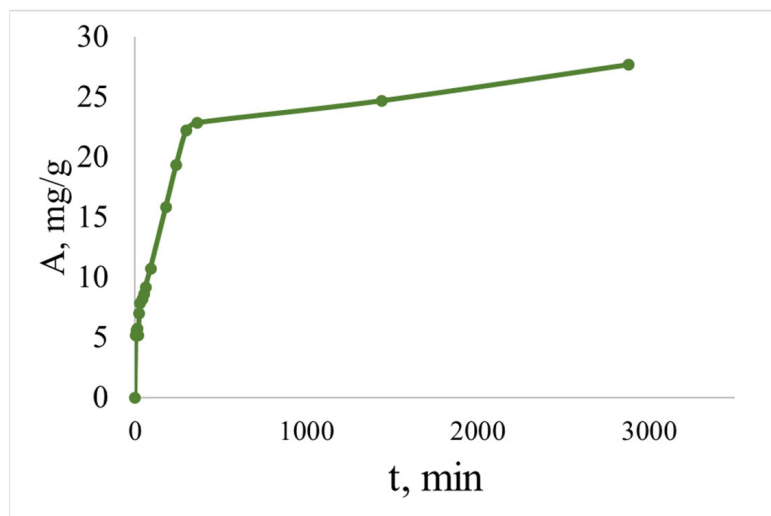


Figure 6. Kinetics of methyl orange sorption using MgCoNi/AlFeY-LDHs from the aqueous solution.

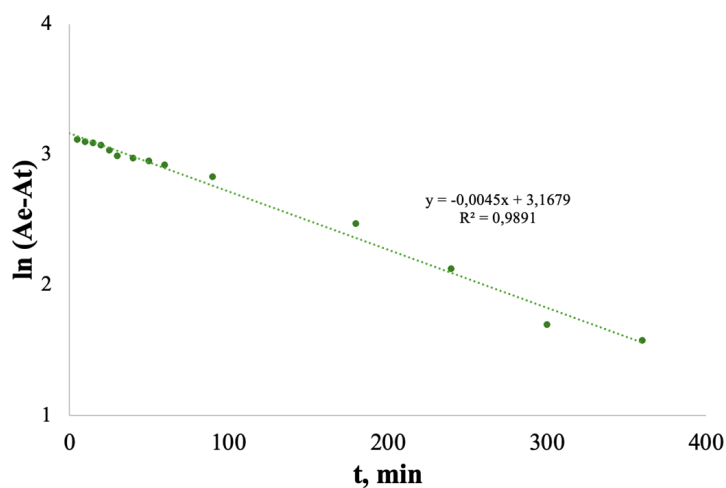


Figure 7. The results of the analysis of methyl orange sorption kinetics using a pseudo-first-order model.

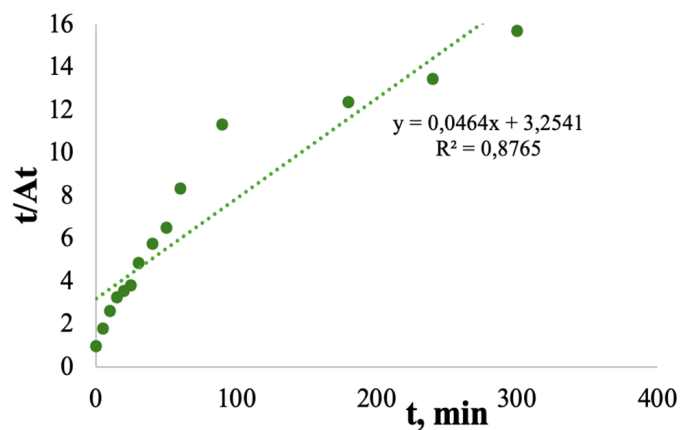


Figure 8. The results of the analysis of methyl orange sorption kinetics using a pseudo-second-order model.

A comparison of the results of using pseudo-first- and pseudo-second-order models to describe the kinetics of the sorption of methyl orange on the synthesized LDHs demonstrates that adsorption is satisfactorily described by the pseudo-first-order model (Figures 7 and 8). As it is known, in the case where the kinetics of the process is described by a pseudo-first-order model, sorption is preceded by diffusion.

Figure 9 shows the sorption isotherm of methyl orange from the synthesized LDHs. The isotherm can be attributed as belonging to the L4 type according to Giles classification [30]. Class L of isotherms is often called the Langmuir class, and the L4 type describes the case of the polymolecular adsorption and/or reorientation of molecules relative to the sorbent surface. In our case, it is also likely that the process begins with surface sorption and is eventually followed by anion exchange.

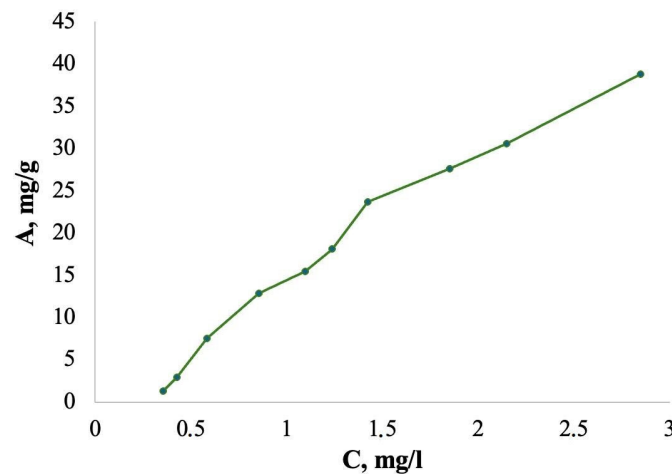


Figure 9. The sorption isotherm of methyl orange from the MgCoNi/AlFeY-LDHs.

To analyze the absorption isotherm in detail, the Langmuir (4) and Freundlich (5) equations were used in their linearized form. The results are presented in Figures 10 and 11.

$$\frac{C_e}{A_t} = \frac{1}{K_1 A_{max}} + \frac{C_e}{A_{max}} \quad (4)$$

$$\lg A_e = \lg K_f + \frac{1}{n} \lg C_e \quad (5)$$

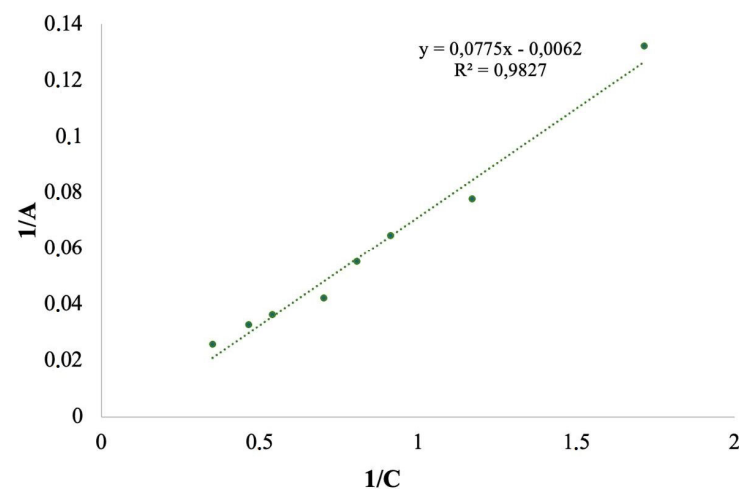


Figure 10. The results of the methyl orange sorption isotherm approximation using the Langmuir equation.

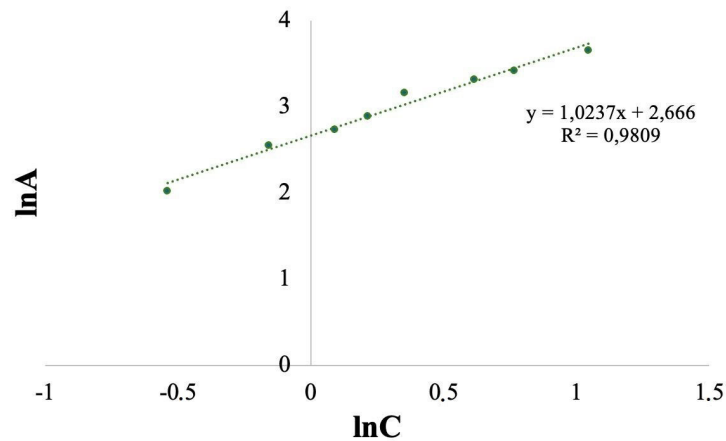


Figure 11. The results of the methyl orange sorption isotherm approximation using the Freundlich equation.

According to the obtained results, one can conclude that the adsorption of methyl orange on the synthesized sample is satisfactorily described by both Langmuir and Freundlich models. Therefore, we can suppose that most of the adsorption centers of LDHs have comparable energy.

The photocatalytic activity of the synthesized sample was evaluated by examining the photolysis of the anionic dye methyl orange. Figure 12 illustrates the kinetic curves for the destruction of methyl orange under UV radiation in the presence of MgCoNi/AlFeY-LDHs. The results indicate that the complete decolorization of the MO solution with MgCoNi/AlFeY-LDHs occurs approximately four times faster than the process without the catalyst.

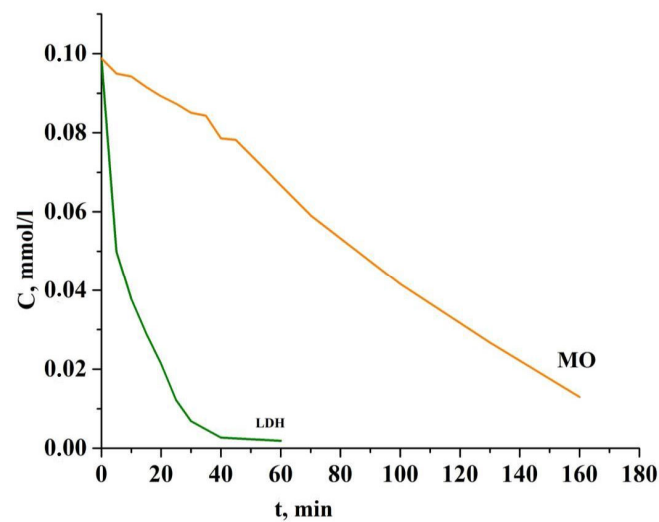


Figure 12. Kinetics of methyl orange destruction under UV irradiation in the presence of MgCoNi/AlFeY-LDHs (LDH curve). For comparison, the MO curve in the absence of LDHs is presented.

Given that layered double hydroxides exhibit high sorption activity, we studied the sorption and photodegradation of MO under identical conditions to assess the effect of sorption in photocatalytic tests. Figure 6 demonstrates that more than 48 h are needed to achieve sorption equilibrium for this sample. Consequently, we can suppose that both sorption and photolysis contribute to the decrease in MO concentration, but the contribution of photodegradation is essential.

4. Conclusions

This study explores the synthesis of high-entropy layered double hydroxides (LDHs) using the mechanochemical method. The developed procedure allows us to make exclusions for stage of ageing under the mother liquor in the LDH synthesis. The activation time, the rotation rate, and the amount of sodium hydroxide were found to affect the crystallinity of LDHs. Optimal conditions for the mechanochemical synthesis were identified to produce single-phase and well-crystallized hexacationic LDHs of the composition MgCoNi/AlFeY with the atomic ratio M^{2+}/M^{3+} approximately equal to 3. The uniform distribution of all cations was confirmed. The calculated value of configurational entropy, excluding inter-layer anions, was 1.43R J/mol·K. The optimal sample demonstrates typical results for LDH XRD patterns, as well as FTIR and Raman spectra, and the ability to absorb anionic dye methyl orange. The sample was shown to possess photocatalytic activity towards methyl orange degradation. Thus, mechanochemical synthesis appears to be a promising approach for obtaining high-entropy layered double hydroxides of any composition, observing the principles of green chemistry.

Author Contributions: Conceptualization, O.K.; methodology, O.K.; formal analysis, M.Y.; investigation, O.K.; resources, M.Y.; writing—original draft preparation, O.K.; writing—review and editing, O.L.; visualization, O.K.; supervision, O.L.; project administration, O.L.; funding acquisition, O.L. All authors have read and agreed to the published version of the manuscript.

Funding: This research was funded by the RSF under grant no. 24-23-00182.

Institutional Review Board Statement: Not applicable.

Informed Consent Statement: Not applicable.

Data Availability Statement: The original contributions presented in this study are included in the article. Further inquiries can be directed to the corresponding author.

Acknowledgments: The authors acknowledge the Joint Research Centre “Technologies and materials” of Belgorod State National Research University for giving the opportunity to use the equipment and for consultations with specialists.

Conflicts of Interest: The authors declare no conflicts of interest.

References

1. Rogachev, A.S. Structure, Stability, and Properties of High-Entropy Alloys. *Phys. Metals Metallogr.* **2020**, *121*, 733. [[CrossRef](#)]
2. Knorpp, A.J.; Zawisza, A.; Huangfu, S.; Borzì, A.; Clark, A.H.; Kata, D.; Graule, T.; Stuer, M. Hydrothermal synthesis of multi-cationic high-entropy layered double hydroxides. *RSC Adv.* **2022**, *12*, 26362. [[CrossRef](#)]
3. Li, H.; Zhou, Y.; Liang, Z.; Ning, H.; Fu, X.; Xu, Z.; Qiu, T.; Xu, W.; Yao, R.; Peng, J. High-Entropy Oxides: Advanced Research on Electrical Properties. *Coatings* **2021**, *11*, 628. [[CrossRef](#)]
4. Novikov, V.; Stepanov, N.; Zherebtsov, S.; Salishchev, G. Structure and Properties of High-Entropy Nitride Coatings. *Metals* **2022**, *12*, 847. [[CrossRef](#)]
5. Li, S.; Tong, L.; Peng, Z.; Zhang, B.; Fu, X. A novel high-entropy sulfide (ZnCoMnFeAlMg)₉S₈ as a low potential and long life electrocatalyst for overall water splitting in experiments and DFT analysis. *Green Chem.* **2024**, *26*, 384–395. [[CrossRef](#)]
6. Storr, B.; Amezaga, C.; Moore, L.; Iwan, S.; Vohra, Y.K.; Chen, C.-C.; Catledge, S.A. High Entropy Borides Synthesized by the Thermal Reduction of Metal Oxides in a Microwave Plasma. *Materials* **2023**, *16*, 4475. [[CrossRef](#)]
7. Miura, A.; Ishiyama, S.; Kubo, D.; Rosero-Nasarro, N.-C.; Tadanaga, K. Synthesis and ionic conductivity of a high-entropy layered hydroxide. *J. Ceram. Soc. Jpn.* **2020**, *128*, 336–339. [[CrossRef](#)]
8. Cavani, F.; Trifiro, F.; Vaccari, A. Hydrotalcite-type anionic clays: Preparation, properties and applications. *Catal. Today* **1991**, *11*, 173–303. [[CrossRef](#)]
9. Evans, D.; Slade, R. Structural Aspects of Layered Double Hydroxides. In *Structure and Bonding*; Springer: Berlin/Heidelberg, Germany, 2005; Volume 119, pp. 1–87.
10. Sels, B.F.; De Vos, D.E.; Jacobs, P.A. Hydrotalcite-like anionic clays in catalytic organic reactions. *Catal. Rev. Sci. Eng.* **2001**, *43*, 443–488. [[CrossRef](#)]

11. Krow, G.R. The Baeyer-Villiger Oxidation of Ketones and Aldehydes. *Org. React.* **2004**, *43*, 251–798.
12. Lin, Y.; Wang, X.; Hao, J.; Ning, P.; Qu, G.; Tang, L.; Xie, Y.; Du, C.; He, Y. Preparation of CuZnAl hydrotalcite-like catalysts for AsH₃ abatement at low temperatures. *Catal. Commun.* **2019**, *118*, 51–55. [[CrossRef](#)]
13. Liang, X.; Zang, Y.; Xu, Y.; Tan, X.; Hou, W.; Wang, L.; Sun, Y. Sorption of metal cations on layered double hydroxides. *Colloids Surf. A Physicochem. Eng. Asp.* **2013**, *433*, 122–131. [[CrossRef](#)]
14. Nestroinaia, O.; Ryl'tsova, I.; Tarasenko, E.; Yapyntsev, M.; Solov'eva, A.; Lebedeva, O. Magnetic materials based on layered double hydroxides. *Pet. Chem.* **2021**, *61*, 388–393. [[CrossRef](#)]
15. Thirunavukkarasu, A.; Nithya, R.; Sivashankar, R. A review on the role of nanomaterials in the removal of organic pollutants from wastewater. *Rev. Environ. Sci. Bio/Technol.* **2020**, *19*, 751–778. [[CrossRef](#)]
16. Naz, S.; Shamoon, M.; Wang, R.; Zhang, L.; Zhou, J.; Chen, J. Advances in therapeutic implications of inorganic drug delivery nano-platforms for cancer. *Int. J. Mol. Sci.* **2019**, *20*, 965. [[CrossRef](#)] [[PubMed](#)]
17. Yasaei, M.; Khakbiz, M.; Ghasemi, E.; Zamanian, A. Synthesis and characterization of ZnAl-NO₃(CO₃) layered double hydroxide: A novel structure for intercalation and release of simvastatin. *Appl. Surf. Sci.* **2019**, *467–468*, 782–791. [[CrossRef](#)]
18. Liu, C.G.; Kankala, R.K.; Liao, H.Y.; Chen, A.Z.; Wang, S.B. Engineered pH-responsive hydrazone-carboxylate complexes-encapsulated 2D matrices for cathepsin-mediated apoptosis in cancer. *J. Biomed. Mater. Res. Part A* **2019**, *107*, 1184–1194. [[CrossRef](#)] [[PubMed](#)]
19. Gu, K.; Zhu, X.; Wang, D.; Zhang, N.; Huang, G.; Li, W.; Long, P.; Tian, J.; Zou, Y.; Wang, Y. Ultrathin defective high entropy layered double hydroxides for electrochemical water oxidation. *J. Energy Chem.* **2021**, *60*, 121–126. [[CrossRef](#)]
20. Zhao, Y.; Ma, H.; Huang, S.; Zhang, X.; Xia, M.; Tang, Y.; Ma, Z.-F. Monolayer Nickel Cobalt Hydroxyl Carbonate for High Performance All-Solid-State Asymmetric Supercapacitors. *ACS Appl. Mater. Interfaces* **2016**, *8*, 22997–23005. [[CrossRef](#)] [[PubMed](#)]
21. Belskaya, O.; Likhobolov, V. Mechanochemical Synthesis of Layered Double Hydroxides as a Promising Method for the Preparation of Adsorbents and Catalysts. *Kinet. Catal.* **2022**, *63*, 615–641. [[CrossRef](#)]
22. Kameliya, J.; Verma, A.; Dutta, P.; Arora, C.; Vyas, S.; Varma, R.S. Layered Double Hydroxide Materials: A Review on Their Preparation, Characterization, and Applications. *Inorganics* **2023**, *11*, 121. [[CrossRef](#)]
23. Nestroinaia, O.V.; Ryl'tsova, I.G.; Lebedeva, O.E. Effect of Synthesis Method on Properties of Layered Double Hydroxides Containing Ni(III). *Crystals* **2021**, *11*, 1429. [[CrossRef](#)]
24. Benito, P.; Guinea, I.; Herrero, M.; Labajos, F.M.; Rives, V. Incidence of Microwave Hydrothermal Treatments on the Crystallinity Properties of Hydrotalcite-like Compounds. *Z. Anorg. Allg. Chem.* **2007**, *633*, 1815–1819. [[CrossRef](#)]
25. Jiang, Y.; Yang, Z.; Su, Q.; Chen, L.; Wu, J.; Meng, J. Preparation of Magnesium-Aluminum Hydrotalcite by Mechanochemical Method and Its Application as Heat Stabilizer in poly(vinyl chloride). *Materials* **2020**, *13*, 5223. [[CrossRef](#)]
26. Bukhtiyarova, M.V. A review on effect of synthesis conditions on the formation of layered double hydroxides. *J. Solid State Chem.* **2019**, *269*, 494–506. [[CrossRef](#)]
27. Rost, C.; Sachet, E.; Borman, T. Entropy-stabilized oxides. *Nat. Commun.* **2015**, *6*, 8485. [[CrossRef](#)] [[PubMed](#)]
28. Lagergren, S. About the theory of so-called adsorption of soluble substance. *Sven. Vetenskapsakademiens Handl.* **1898**, *24*, 147–156.
29. Ho, Y.S.; McKay, G. Pseudo-second order model for sorption processes. *Process Biochem.* **1999**, *34*, 451–465. [[CrossRef](#)]
30. Giles, C.; MacEwan, T.; Nakhwa, S.; Smith, D. Studies in adsorption: A system of classification of solution adsorption isotherms. *J. Chem. Soc.* **1960**, *3*, 3973–3993. [[CrossRef](#)]

Disclaimer/Publisher's Note: The statements, opinions and data contained in all publications are solely those of the individual author(s) and contributor(s) and not of MDPI and/or the editor(s). MDPI and/or the editor(s) disclaim responsibility for any injury to people or property resulting from any ideas, methods, instructions or products referred to in the content.